Proceedings of the 11th ICPMG 2026
11th International Conference on Physical Modelling in Geotechnics
8-12 June 2026, Zurich, Switzerland

Development and experimental validation of an energy-based evaluation method for pile construction in dry Toyoura sand

Nana Shinhara
Graduate student, Graduate School of Science and Engineering, Chuo University, Tokyo, Japan
a22.f7tt@g.chuo-u.ac.jp

Tomoya Haraguchi
Graduate student, Graduate School of Science and Engineering, Chuo University, Tokyo, Japan
a22.meaa@g.chuo-u.ac.jp

Hidetoshi Nishioka
Professor, Faculty of Science and Engineering, Chuo University, Tokyo, Japan
nishioka@civi.chuo-u.ac.jp

ABSTRACT: Pile foundation construction methods have traditionally been selected based on empirical rules, and an energy-based quantitative evaluation framework remains to be established. A notable bottleneck is the scarcity of model experiments capable of isolating and reproducibly simulating the mechanical processes involved in actual construction. Therefore, this study was aimed at conducting fundamental model experiments to clarify the relationship between lateral resistance and installation energy in pile foundations. All experiments were performed under gravitational (1g) conditions using dry Toyoura sand. Two forms of energy were examined: installation energy required for pile penetration, and resistance energy accumulated in the pile–soil system during lateral loading. Installation energy was calculated as the work done by the press-in machine during installation for piles with different specifications. After installation, monotonic lateral displacement was applied at the pile head, and resistance energy was evaluated as the energy stored in the pile–soil system, obtained from the load–displacement relationship. The installation energy increased rapidly with the dimensionless parameter βL, and the energy required to achieve the same penetration depth differed depending on pile type and cross-sectional shape. Although the resistance energy also increased with βL, its increase rate diminished beyond a threshold, and this transition point depended on pile type. Energy efficiency was calculated as the ratio of the installation energy to the resistance energy, and its maximum value was observed at a specific βL value. As this study was conducted under 1g conditions, the stress state may differ from that in actual field construction. Nevertheless, the proposed approach provides a rational, energy-based mechanical framework for evaluating pile construction. Rather than relying on conventional empirical judgement, it offers an experimental foundation for the systematic assessment and comparison of different pile installation methods.

1 RESEARCH BACKGROUND

The construction of pile foundations requires substantial energy. Even for piles with identical diameters and lengths, the energy demand varies depending on the installation method, resulting in differing levels of energy efficiency across construction techniques. In urban projects, pile specifications, such as diameter, length, and number, and installation methods have traditionally been selected based on economic considerations informed by past construction records, as well as environmental constraints such as noise and vibration. Thus, although energy efficiency has been implicitly considered through cost evaluations, it has rarely been examined directly as a mechanical performance indicator.

In recent years, however, pile construction has expanded into remote and challenging environments, including offshore wind turbine foundations and large-scale solar power generation facilities in desert regions. From a forward-looking perspective, developments in space exploration suggest that pile construction techniques may eventually be required on the Moon or Mars. In such settings, where construction experience is limited and environmental constraints differ from those in the habitable land area on Earth, a mechanical assessment of energy efficiency is critical.

A representative contribution in this area is the work of Gómez et al. (2022), who evaluated the driving efficiency of vibratory piles for offshore wind monopiles based on the energy input from a vibratory driver. Nonetheless, only a limited number of studies have directly compared the energy consumed during construction with the lateral resistance performance of the installed pile.

To address this gap, the present study conducted fundamental model experiments under gravitational conditions using dry Toyoura sand to qualitatively investigate the relationship between installation energy and lateral-resistance energy for pile foundations. The press-in method was adopted as the installation technique. This method employs hydraulic jacks to install piles statically, without impact or vibration, thereby minimising disturbance to the surrounding ground. White et al. (2002) demonstrated that noise and ground vibrations during installation are significantly reduced when using the press-in method compared with conventional impact driving. Given these advantages, press-in techniques have been widely adopted in Japan, particularly in urban areas and near existing structures. More recently, Gavin and Duffy (2024) highlighted their potential applicability in the offshore renewable energy sector.

In this study, the energy input during construction (installation energy) and energy stored in the pile–soil system during lateral loading (resistance energy) were measured to examine their qualitative relationship, thereby providing an energy-based perspective for evaluating pile construction. Three types of piles with different cross-sectional shapes and dimensions were employed to investigate how variations in pile specifications influence this energy relationship.

2 EXPERIMENT SUMMARY

2.1 Model ground and model pile

Figure 1 illustrates the ground model used in the experiments. Dry Toyoura sand served as the ground material. Toyoura sand is a natural silica sand characterised by a uniform particle-size distribution and excellent reproducibility, and it is thus widely used in geotechnical model experiments in Japan.

The model ground was prepared by pluviating sand to a height of 400 mm inside a soil container with a width of 1000 mm and depth of 450 mm. An air-pluviation device equipped with multiple sieves was used to ensure uniform deposition. The container dimensions were selected to minimise boundary effects on the experimental results.

As shown in Figure 2, two types of phosphor-bronze plates with different thicknesses and one acrylic pipe were used as model piles. All piles had a total length of 500 mm. The detailed dimensions and material properties are summarised in Table 1.

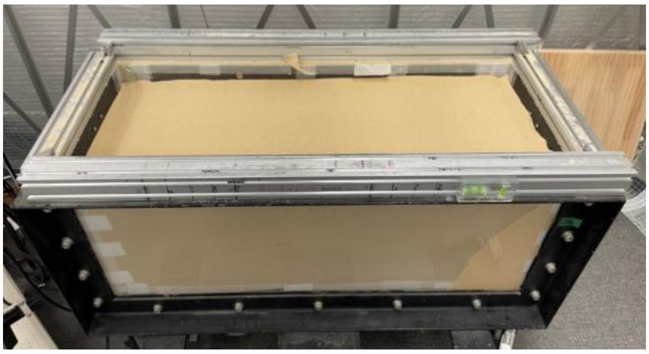

Figure 1. Model ground

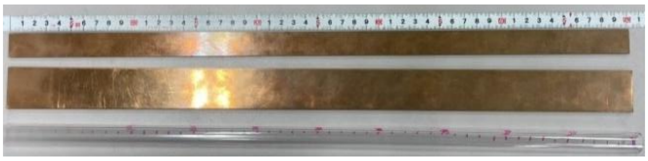

Figure 2. Model piles

Table 1. Pile Parameters

Pile type	Plate pile		Pipe pile
Material	Phosphor bronze		Acrylic
***E*: Young's modulus (GPa)**	110		3.2
***t*: Thickness (mm)**	2	3	2
***B*: Width or Diameter (mm)**	20	33	15
***A*: Cross-sectional area (mm²)**	40	99	81.6
Length (mm)	500		
***EI*: Bending stiffness (N・m²)**	1.47	8.17	5.65

2.2 Experimental methods

Figure 3 illustrates the experimental apparatus used for the press-in and lateral-loading experiments. In the press-in process, as shown in Figure 3(a), each model pile was initially placed in the soil container and allowed to settle under its self-weight, with a mass of 0.91 kg applied at the pile head. After natural penetration ceased, the weight was removed, and the pile was pressed into the ground at a constant rate of 1.0 mm/s using an electric actuator.

During installation, the axial force at the pile head was measured using a load cell attached to the actuator, hereafter referred to as the press-in force. The vertical displacement was monitored using a wire-type

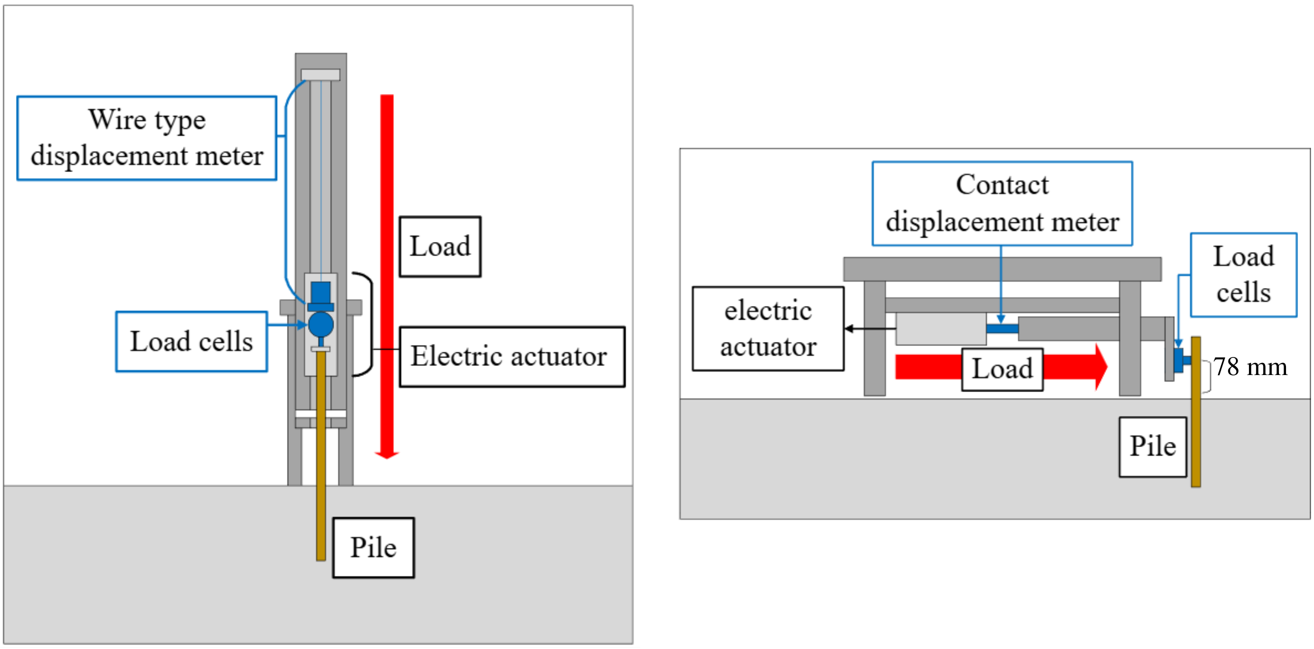

a) *Press-in apparatus*

b) *Lateral-loading apparatus*

Figure 3. Schematic of experimental setup

displacement transducer. A guiding mechanism was used to maintain vertical alignment and ensure penetration parallel to the container wall.

In the remaining paper, the vertical displacement of the model pile during installation is defined as the penetration length l, and the cumulative penetration at the end of installation is referred to as the embedment depth L. These measurements helped clarify the relationship between the press-in force and penetration length. Preliminary experiments confirmed that variations in press-in velocity did not influence the results.

Following installation, lateral-loading experiments were performed using the setup shown in Figure 3(b). The electric actuator applied quasi-static lateral displacement at a constant rate of 0.04 mm/s at a loading point located 78 mm above the ground surface. Loading was continued until a displacement of 5 mm was reached.

The lateral load was measured using a load cell attached at the loading point, and the displacement was recorded using a contact-type displacement transducer.

2.3 Experimental case

A total of 12 cases were established by varying the embedment depth L for each pile type. Pile installation was terminated when the pile reached the prescribed L.

Table 2. Experimental cases

Pile type	Plate pile		Pipe pile
B: Width or diameter (mm)	20	33	15
A: Cross-sectional area (mm^2)	40	99	81.6
L: Embedment depth (mm)	100	100	90
	120	110	100
	130	130	110
	150	140	120
	160	160	130
	180	170	140
	190	190	150
	210	200	160
	240	220	170
	250	230	180
	270	250	190
	280	260	210

3 EXPERIMENTAL RESULTS

3.1 Press-in experiment results

Figure 4 shows the relationship between the press-in force and penetration length l obtained from the press-in experiments.

Under identical ground conditions, experiments using plate and pipe piles of different sizes showed that for the plate piles, the required press-in force increased with a larger cross-sectional area A. In contrast, the pipe pile required a substantially larger press-in force than the plate piles, even those with a larger material cross-sectional area (e.g., B = 33 mm, A = 99 mm^2). This behaviour is attributable to the 'plugging effect', where sand fills the hollow section of the pipe during penetration. Consequently, the pipe pile behaves as a solid pile, increasing its resistance area beyond the actual cross-section of the pipe material itself. This leads to a substantial increase in tip resistance and explains why the press-in force for the pipe pile exceeds that of the plate piles with larger cross-sections.

Regarding the overall trend of press-in force, the plate piles showed little variation with penetration length l. In contrast, the pipe pile displayed greater fluctuations. This behaviour is likely caused by pre-buckling deformations in the pipe pile during press-in, which temporarily disrupt the equilibrium between the press-in force and soil reaction, leading to scattered increases in the measured force.

3.2 Lateral load experiment results

Figure 5 shows the relationship between lateral load and displacement at the pile head, obtained from the lateral loading experiments conducted after the press-in process. All pile types exhibited nonlinear behaviour, with the rate of increase in lateral load decreasing as displacement increased. In addition, the

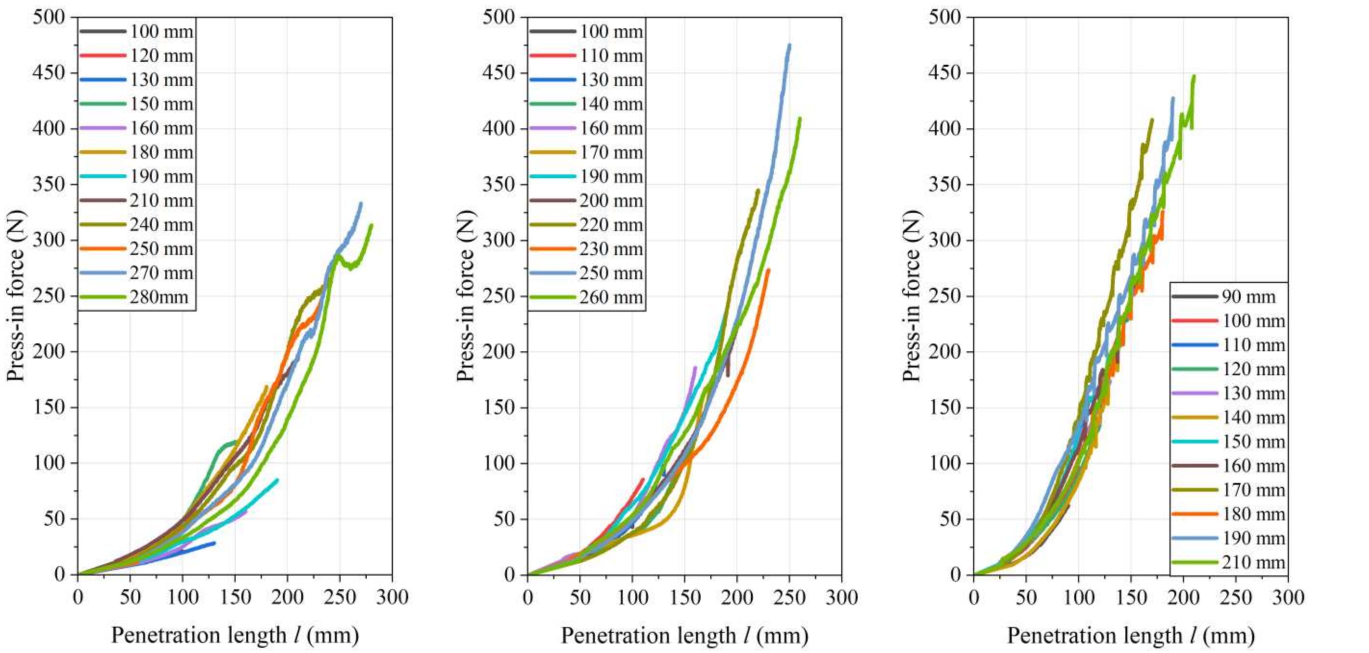

a) Plate pile
(B = 20 mm, A = 40 mm²)

b) Plate pile
(B = 33 mm, A = 99 mm²)

c) Pipe pile
(B = 15 mm, A = 81.6 mm²)

Figure 4. Relationship between the press-in force and penetration length l

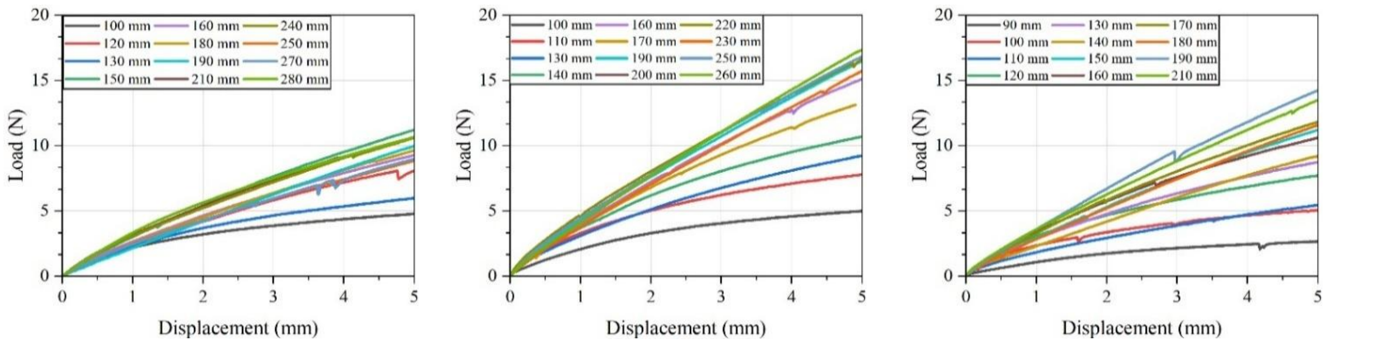

a) Plate pile
(B = 20 mm, A = 40 mm²)

b) Plate pile
(B = 33 mm, A = 99 mm²)

c) Pipe pile
(B = 15 mm, A = 81.6 mm²)

Figure 5. Lateral loading experiment results

Table 3. Results of β calculation

Pile type	**B**: Width or diameter (mm)	*A:* Cross-sectional area (mm^2)	β (m^{-1})	1/β (mm)
Plate pile	20	40	13.8	72.5
	33	99	10.4	96.4
Pipe pile	15	81.6	13.8	72.5

lateral resistance decreased with decreasing embedment depth L.

For all model piles, no residual deformation was observed before or after the experiments, indicating that the piles remained within the elastic range. Consequently, the lateral load at the pile head is considered to have been generated primarily by the plastic deformation of the surrounding soil.

To compare model piles with varying bending stiffness EI, the results were normalised using the dimensionless parameter βL, defined as the product of the penetration length L and characteristic parameter β (Chang, 1937). As shown in Eq. (1), β is a dimensionless parameter representing the stiffness ratio between the pile and soil, enabling comparisons across different pile diameters and soil conditions. For all pile types, β was back-calculated using Eq. (2) based on the lateral load at a displacement of 1 mm, specifically for the experimental cases with an embedment length of 190 mm. The resulting values are summarised in Table 3.

$$y_t = \frac{(1+\beta \cdot h)^3 + \frac{1}{2}}{3EI \cdot \beta^3} \cdot H \tag{1}$$

$$\beta = \sqrt[4]{\frac{K_h \cdot B}{4EI}} \tag{2}$$

where β (mm^{-1}) is a key parameter of the pile–soil system, K_h is the coefficient of the lateral subgrade reaction, B (mm) is the pile width or diameter, y_t (mm) is the lateral displacement at the loading point, H (N) is the applied lateral load, EI (N·m) is the bending stiffness, and h (mm) is the height of the loading point.

3.3 Energy calculation

The installation energy E_I was defined as the work performed by the weight and press-in machine on the model pile. Based on the relationship between press-in force and penetration length l shown in Figure 4, the installation energy was calculated using Eq. (3):

$$E_I = \int_0^L P_C(l)dl \tag{3}$$

where E_I (mJ) is the installation energy; P_C (N) is press-in force at penetration length l, including the initial penetration caused by the weight; and L (mm) is a specified embedment depth.

The resistance energy E_R is defined as the energy stored in the pile–soil system during lateral loading. It was evaluated as the area enclosed by the load–

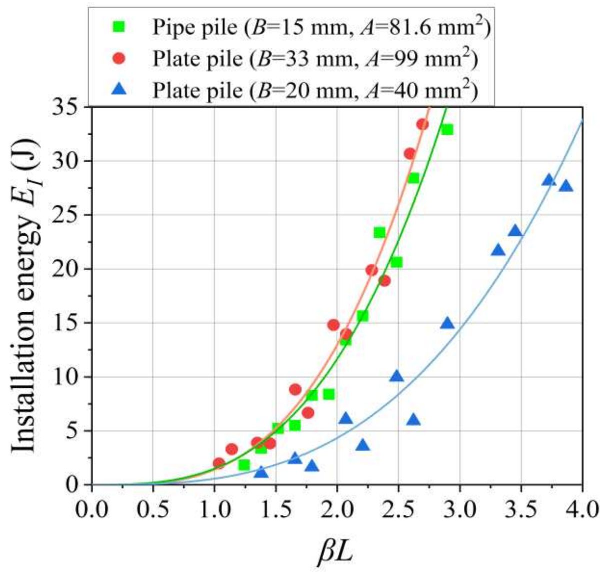

Figure 6. Relationship between installation energy E_I and βL

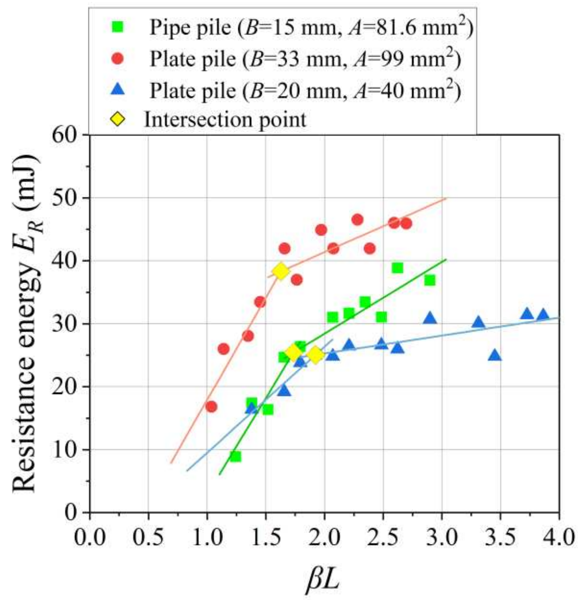

Figure 7. Relationship between resistance energy E_R and βL

Table 4. Approximate formula for installation energy

Pile type	Plate pile		Pipe pile
B: Width or diameter (mm)	20	33	15
A: Cross-sectional area (mm^2)	40	99	81.6
Approximation formula	$E_I = a(\beta L)^2 + b(\beta L)^3$		
a	54.2	-420.0	72.7
b	515.2	1831.9	1421.7
R²	0.96	0.98	0.96

displacement curve up to a displacement of 5 mm (Figure 5), as expressed in Eq. (4):

$$E_R = \int_0^{5\mathrm{mm}} P_R(x)dx \quad (4)$$

where E_R (mJ) is the resistance energy and $P_R(x)$ (N) is the lateral resistance force at displacement x.

Figure 6 shows the relationship between installation energy E_I and βL, while Figure 7 presents the relationship between resistance energy E_R and βL. Both E_I and E_R increased with increasing βL, although the trends differed between the two energy types.

To qualitatively compare these trends, approximation curves were fitted to the experimental data. E_I was approximated using a cubic function, reflecting the quadratic behaviour of the relationship between press-in force and penetration length l, considering the fact that E_I is the integral of this press-in force with respect to penetration length l.

In contrast, as E_R exhibited a distinct change in slope, the data for each pile type were divided at an optimal point into two segments, each fitted with a linear function. This division point was determined through trial and error to maximise the coefficients of determination R^2 for both segments. Denoting the βL value at the intersection of the two linear segments as βL_r, the results indicate that βL_r decreases as the pile stiffness increases. The approximation equations and corresponding R^2 values for the installation and resistance, along with the βL_r values, are summarised in Tables 4 and 5, respectively.

Figure 8 illustrates the relationship between the calculated installation energy E_I and resistance energy E_R. The plot presents both experimental results and the curves derived from the approximation equations for both energy types. The results indicate that beyond a certain threshold, further increases in E_I (i.e., embedment depth L) result in only limited gains in resistance energy, demonstrating a region of diminishing returns. Furthermore, comparison among

Table 5. Approximate formula for resistance energy

Pile type	Plate pile		Pipe pile
B: Width or diameter (mm)	20	33	15
A: Cross-sectional area (mm^2)	40	99	81.6
Approximation formula	$E_R = c(\beta L) + d$		
c	-7.32	-14.5	-27.7
d	16.8	32.5	30.6
R²	0.90	0.74	0.90
βL_r (mm)	1.92	1.63	1.74
Approximation formula	$E_R = e(\beta L) + f$		
e	19.6	24.9	5.6
f	2.8	8.3	11.4
R²	0.45	0.62	0.72

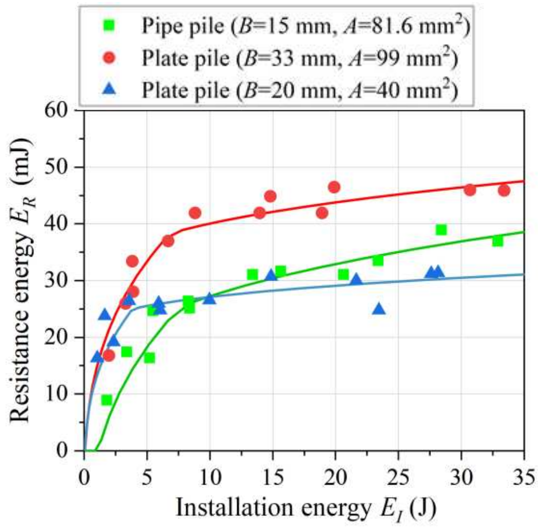

Figure 8. Relationship between installation energy E_I and resistance energy E_R

different pile geometries reveals that the E_I required to achieve a given E_R varies depending on the pile type and cross-sectional configuration. Piles with higher bending stiffness are found to more efficiently convert the input construction energy into resistance energy. In contrast, for the open-ended pipe pile, the resistance energy continues to increase even as the embedment depth L grows. As previously discussed, this behaviour is likely attributable to the plugging effect, which causes the open-ended pile to behave similarly to a solid (closed-ended) pile, leading to a continuous gain in resistance.

3.4 Calculation of energy efficiency

The total construction energy E_C expended during pile installation includes not only the installation energy E_I supplied by the press-in machine but also the energy associated with material manufacturing, as well as the transport and operation of equipment and materials. These contributions are collectively defined as the preparation energy, E_P. Energy efficiency λ is then defined by Eq. (5) as the ratio of resistance energy E_R to the total construction energy $E_C = E_I + E_P$. Here, the evaluation assumes that the preparation energy E_P can be quantified independently, and energy efficiency is estimated based on this assumption.

$$\lambda = \frac{E_R}{E_C} = \frac{E_R}{E_I + E_P} \tag{5}$$

where E_R (mJ) is the resistance energy, E_C (mJ) is the total construction energy, E_I (mJ) is the installation energy, and E_P (mJ) is the preparation energy.

For estimation, the preparation energy per pile, E is assumed to scale approximately linearly with the installation energy E_{Ir} corresponding to βL_r, i.e., the intersection points of the two-segment approximation of the E_R–βL relationship (Table 6). Based on this assumption, E_P is calculated using Eq. (6), where α represents the preparation energy ratio.

$$E_P = \alpha \cdot E_{Ir} \tag{6}$$

Figure 9 presents the relationship between energy efficiency λ and βL, calculated from the experimental the results while incorporating the preparation energy ratio α. The values of α are varied as 0.1, 1.0, and 10. When α = 0.1, the energy efficiency λ reaches its maximum at a βL value below βL_r. For $\alpha \geq 1$, except for the pipe pile, the energy efficiency λ peaks near βL_r, and further increases in α do not shift the βL corresponding to the maximum value. In the case of the pipe pile, however, the βL corresponding to the maximum λ increases as α increases. A common trend

Table 6. Values of βL_r and the corresponding installation energy E_{Ir} and resistance energy E_{Rr}.

Pile type	Plate pile		Pipe pile
***B*: Width or diameter (mm)**	20	33	15
***A*: Cross-sectional area (mm^2)**	40	99	81.6
βL_r	1.92	1.63	1.74
E_{Ir}: Installation energy (mJ)	3864	6800	7657
E_{Rr}: Resistance energy (mJ)	25.1	38.3	25.4

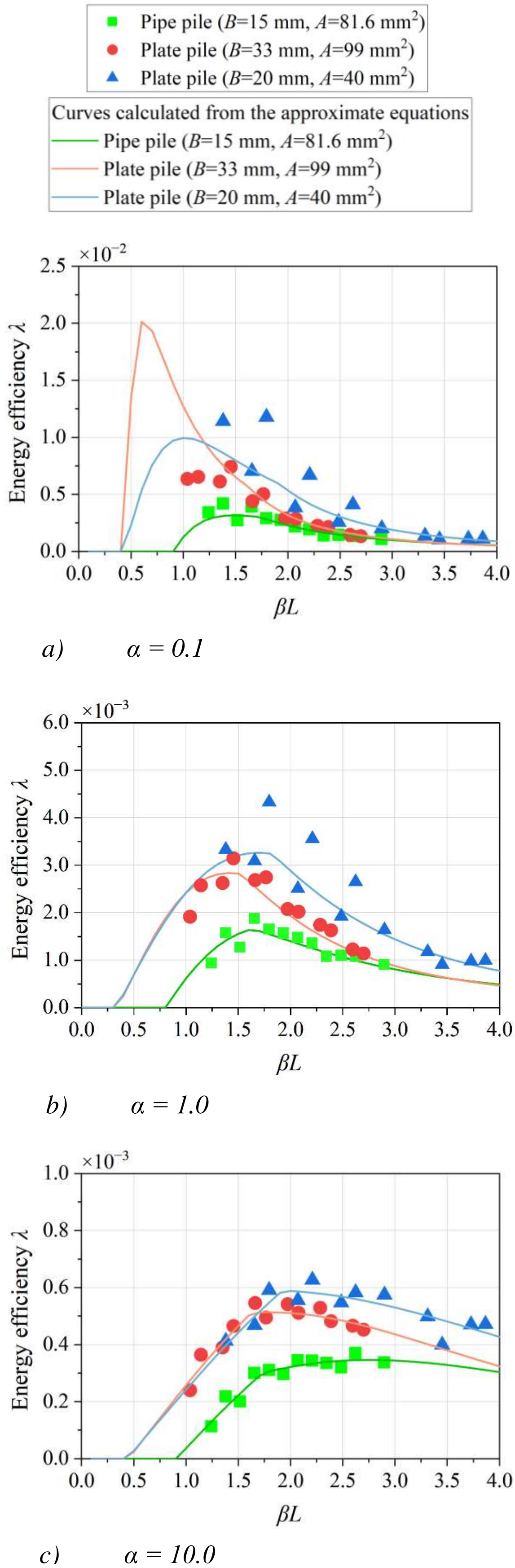

Figure 9. Relationship between energy efficiency λ and βL

observed across all piles is that the decrease in energy efficiency beyond βL_r becomes more gradual.

These results indicate that λ is strongly influenced by the magnitude of E_P, and that the βL corresponding to the maximum efficiency varies with α. At construction sites equipped with high-performance machinery capable of installing multiple piles efficiently, the preparation energy per pile can be reduced, making shorter, stiffer piles more efficient. Conversely, in environments such as the lunar surface, where preparation energy is extremely high, installing piles near βL_r is expected to yield higher energy efficiency. It should be noted that actual construction involves additional energy losses not reproduced in the model experiments, such as mechanical friction and vibration-related losses, which must be considered separately.

The experiments in this study were conducted under 1g conditions; therefore, the stress state differs from that of actual field construction. This renders it challenging to directly apply the coefficients of the derived approximate equations and numerical results to real-scale field conditions. However, this study clarified the fundamental mechanisms of how construction energy and resistance energy change in response to variations in pile specifications, in addition to the embedment depth. Based on these findings, a qualitative mechanical framework was proposed to explain the relationship between pile specifications and energy efficiency in the press-in method.

Furthermore, although the present study focused on the press-in method, the proposed energy-based evaluation approach can serve as a general framework for assessing the energy efficiency of other construction methods, such as impact driving. Consequently, the results of this study provide foundational insights for understanding how differences in construction conditions affect energy efficiency, providing a qualitative conceptual foundation rather than a strictly quantitative prediction.

4 CONCLUSION

Press-in and lateral loading experiments were conducted using model piles with various bending stiffnesses and cross-sectional shapes to evaluate construction efficiency in terms of installation energy E_I and resistance energy E_R. The results demonstrated that piles with larger cross-sectional areas, as well as pipe piles where the plugging effect considerably enhances tip resistance, require larger E_I for a given embedment depth L. By approximating the relationship between E_R and the dimensionless parameter βL with bi-linear segments, the intersection point βL_r was identified. The evaluation revealed that stiffer piles reach this critical efficiency point at shorter embedment lengths, suggesting that increasing stiffness is an effective strategy for mobilising resistance energy more rapidly.

Furthermore, the evaluation of energy efficiency λ revealed that the optimal βL for maximum efficiency depends strongly on the preparation energy ratio α. While lower α values favour smaller βL, environments with extremely high preparation costs make designing near βL_r most effective for maximising efficiency. This indicates that the ideal pile specification varies significantly according to the logistics and operational overhead of the construction site.

Although the 1g model experiments involve stress states different from actual field conditions, this study clarifies the fundamental mechanics of how pile specifications influence energy balance. Consequently, the proposed qualitative framework provides essential basic information for optimising pile design and construction efficiency across diverse environments, taking into account the balance between installation, preparation, and resistance energies.

Future work will include comparisons with other construction methods. For example, model experiments simulating the conventional impact driving method using a falling weight will be performed, enabling a systematic comparison of installation energy and resistance energy across different construction techniques. This will help establish a foundation for qualitatively evaluating differences in energy efficiency among various pile installation methods.

REFERENCES

Chang, Y.L. (1937). Discussion on “Lateral pile-loading tests” by L. B. Feagin. *Transactions of the American Society of Civil Engineers*, 102(1): 272–278. https://doi.org/10.1061/TACEAT.0004849

Gavin, K. and Duffy, K. (2024). The potential use of press-in methods in the offshore renewables industry. *Proceedings of the 3rd International Conference on Press-in Engineering 2024*, Singapore.

Gómez, J., Tsetas, D., and Metrikine, A. (2022). Energy flux analysis for quantification of vibratory pile driving efficiency. *Soil Dynamics and Earthquake Engineering,* 158: 107312. https://doi.org/10.1016/j.jsv.2022.117299

White, D.J. Bolton, M.D., and Bearss, G. (2002). Press-in piling: Ground vibration and noise during pile installation. *Proceedings of the Institution of Civil Engineers – Geotechnical Engineering*, 155(4): 187–195. https://doi.org/10.1061/40601(256)26